processes

MDPI

Article

Au-Pd Bimetallic Nanocatalysts Incorporated into Carbon Nanotubes (CNTs) for Selective Oxidation of Alkenes and Alcohol

Hamed M. Alshammari [1,*], Abdullah S. Alshammari [2], Jamal R. Humaidi [1], Salma A. Alzahrani [1], Mosaed S. Alhumaimess [3], Obaid F. Aldosari [4] and Hassan M. A. Hassan [3,5]

1 Chemistry Department, Faculty of Science, University of Ha'il, P.O. Box 2440, Ha'il 81451, Saudi Arabia; j.humaidi@uoh.edu.sa (J.R.H.); s.alzahrane@uoh.edu.sa (S.A.A.)
2 Physics Department, Faculty of Science, University of Ha'il, P.O. Box 2440, Ha'il 81451, Saudi Arabia; a.alshamri@uoh.edu.sa
3 Chemistry Department, College of Science, Jouf University, P.O. Box 2014, Sakaka 72341, Saudi Arabia; mosaed@ju.edu.sa (M.S.A.); hmahmed@ju.edu.sa (H.M.A.H.)
4 Department of Chemistry, College of Science, Majmaah University, P.O. Box 66, Majmaah 11952, Saudi Arabia; O.Aldosari@mu.edu.sa
5 Department of Chemistry, Faculty of Science, Suez University, Suez 43511, Egypt
* Correspondence: h.alshammari@uoh.edu.sa

Received: 5 September 2020; Accepted: 26 October 2020; Published: 30 October 2020



Abstract: Although supported bimetallic nanoparticles (Au-Pd NPs) demonstrate outstanding efficiency, challenges appear for carbon supported small and stable bimetallic nanoparticles used in liquid-phase reactions. In this work, Au-Pd NPs were supported on two types of carbon nanotubes: CNTs decorated covalently with carboxylic acid groups (O-CNTs) and non-covalently with the conductive poly(3,4-ethylenedioxythiophene) polystyrene sulfonate (PEDOT:PSS) polymer (P-CNTs). The Au-Pd NPs were prepared using the sol immobilization approach on the functionalized CNTs, and the effect of the utilized functionalization method on the properties of the immobilized metallic nanoparticles and the performance of the nanocomposite catalysts was investigated. The fabricated nanocomposites were characterized using Fourier-transform infrared spectroscopy (FTIR), Raman spectroscopy, High-resolution transmission electron microscopy (HRTEM) and scanning electron microscopy (SEM). The catalytic performance of Au-Pd/O-CNTs and Au-Pd/P-CNTs was exploited for the oxidation of both cyclooctene and benzyl alcohol. Oxidation and polymer decoration directly led to an enhancement in the performance of CNTs catalysts. The nanocomposite catalyst with oxidized CNTs (Au-Pd/O-CNTs) was also found to be much more efficient and robust than that with polymer decorated CNTs (Au-Pd/P-CNTs). The enhancement in the oxidation of both cyclooctene and benzyl alcohol on Au-Pd/O-CNTs is attributed to the well-dispersed and smaller Au-Pd NPs as active sites on the surface of O-CNTs as compared to the P-CNTs surface.

Keywords: Au-Pd nanocatalysts; carbon nanotubes; oxidation reaction

1. Introduction

Controlled morphology and composition of the metallic and multimetallic nanomaterials have gained great interest due to of their exceptional catalytic efficiency in various fields including petroleum-refining substances, production of hydrogen and other various major chemical reactions [1–4]. Among these metallic nanoparticles, gold and palladium have played a very important role in the catalysis processes [5,6]. The bimetallic systems of Au-Pd have been used for several reactions including CO oxidations at low temperatures, reduction of NO, direct generation of H_2O_2 from the O_2 + H_2

reaction mixture and vinyl acetate synthesis [7–10]. The design of an efficient catalyst relies on the structure-performance relationship, the fabrication of the catalysts with well-defined structures and the factors that govern the catalytic performance of the synthesized catalyst [11–13]. Moreover, it is well documented that the support of the bimetallic nanocatalysts has a role in the improvement of the catalytic performances of the nanostructures [14–16]. Supported metallic catalysts such as Au, Pd, Pt, Ru and bimetallic catalysts have shown considerable progress in the conversion of hydroxymethylfurfural to furan dicarboxylic acid using air or molecular oxygen (O_2) as a catalyst [17–19]. Supported gold catalysts particularly have acquired a major interest owing to their great performance in the oxidation of 5-hydroxymethylfurfural to 2,5-furan dicarboxylic acid and their resistance to oxide formation as well as catalytic oxidation of various organic materials [20]. Gold nanoparticles themselves have shown remarkable properties because of their high conductivity, biocompatibility, large surface area and high surface energy, which make gold nanoparticles key catalysts in various organic reactions, sensing and biomedical applications [21,22]. Palladium also is among the most potent metallic catalysts in the chemical industries. Its capability of catalyzing the C-C bond formation and the stability of several Pd based-catalysts to water or oxygen are two of the main reasons for its significance. As a catalyst in hydrogenation reactions, Pd is especially effective. Furthermore, when supported, these metal catalysts achieve a much greater performance. This is because particles from the metallic catalyst could be more widely distributed and are, therefore, exposed to a higher proportion of reactants. Up to 75% of the hydrogenation processes are currently carried out utilizing C catalysts [23]. Benzyl alcohol oxidation, owing to the need for benzaldehyde as an intermediate in the manufacture of fine chemicals and flavoring ingredients, is one of the most important alcohol oxidation process in the industry. In addition, epoxidation of unsaturated compounds, as epoxides provide a direct approach to a range of materials, is an interesting field of academic and industrial fields. The use of heterogeneous catalysts in the catalytic oxo-functionalization of aromatic and aliphatic alkenes for the development of various worthy chemicals such as alcohols, ketones, peroxides and acids have been proven advantageous over homogenous catalytic systems because of their recoverable nature and the use of eco-friendly conditions like the use of H_2O_2 or molecular oxygen as a mild oxidants [24].

Carbon based-nanomaterials, on the other hand, like carbon nanotubes (CNTs) and nanofibers, are a promising catalyst support for metal nanomaterials because of their complete recoverable nature, great stability in aqueous solution over an expansive pH range and ease of their surface functionality by integrating other elements. Additionally, they have found various applications in fuel cell catalysis, catalysis in aqueous phases and they function as a main ingredient in electronic and energy materials, sensors and catalysis [25–27]. Carbon nanotubes, in particular, are considered to be very promising candidates for catalysis applications. In fact, metallic NPs-supported CNTs based catalysts have demonstrated numerous advantages including high catalytic performance and durability. Therefore, metallic NPs/CNTs systems could have many promising applications in various fields including highly efficient optical electronics, sensors, heterogeneous catalysis and electrocatalysis [28]. Previous researches of metallic nanoparticle catalysts supported carbon-based materials have revealed that carbon surface features affect both the size of the metallic nanoparticles and the catalysts efficiency [29]. In some cases, however, the observed catalytic effects could not be ascribed solely to carbon surface properties as catalysts, but are also associated with various metallic particle sizes and distributions. The great surface area of carbon nanotubes (CNTs) provides many nucleation sites when noble metallic nanoparticles are bound to carbon nanotubes, thus decreasing the need for a capping-agent to regulate the size of the particles and to hinder the non-uniform particles growth. Besides, the synergistic effect is generally attributed to the integration effect assigned to the regional structure of Au-Pd and the electronic impact that might affect the catalytic performance. However, although many studies have investigated the catalytic performance of various CNTs supported metallic nanoparticles, it is very rare to find reports that discuss the effect of the side-wall modification of CNTs, which is essential for CNTs dispersion, on the growth of metallic NPs and the performance of the produced catalysts. Therefore, in this study, we described in details the

immobilization of Au-Pd on carbon nanotubes with different surface functionalities to improve the catalytic activity of the as-synthesized supported catalyst. We also investigated the effect of the different CNTs functionalization methods on the morphological properties of the immobilized nanoparticles and the performance of the developed nanocomposite catalysts for the selective oxidation of alkenes and alcohol.

2. Materials and Methods

2.1. CNTs Functionalizations

Two groups of multi-wall carbon nanotubes (MWCNTs, purchased from Sigma-Aldrich, Dorset, UK) were prepared and used in the current study. The first CNTs group was covalently functionalized with carboxylic acid groups and the second one was non-covalently functionalized with the conductive PEDOT: PSS polymer (Sigma-Aldrich, UK). The details of carboxylic acid and conductive polymer functionalizations of CNTs are reported in previous works [30–33]. Briefly, covalent functionalization of CNTs with carboxylic acid groups was performed by adding CNTs to a 1:3 mixture of nitric acid and sulfuric acid. The blend was left for about 10 min under continuous sonication and was then refluxed at 130 °C for about 1 h. After that, the CNTs-acid blend was diluted with deionized DI water and centrifuged several times in order to obtain a stable suspension of well dispersed nanotubes. Moreover, to functionalized CNTs with the conductive PEDOT: PSS polymer, CNTs were first dispersed in DI water using a powerful sonication probe and then PEDOT: PSS was added slowly to CNTs suspension under continuous sonication for about 30 min. The PEDOT: PSS functionalized CNTs suspension was then centrifuged several times to obtain stable CNTs dispersion.

2.2. Catalyst Preparation

This research work aims to prepare and evaluate the performance of Au-Pd catalyst that is deposited on CNTs functionalized by different approaches. To recognize the drive and development of this research, emphasis is given here on the significant catalyst preparation parameters. The detailed catalyst fabrication recipe is reported in the literature [34]. Typically, 1 wt % of Au:Pd catalyst was synthesized employing a $PdCl_2$ (6 mg in 1 mL) and $HAuCl_4 \cdot 3H_2O$ (12.25 g in 1000 mL) aqueous solution. Gold and palladium solutions were then agitated for 15 min in distilled water and followed by adding polyvinyl alcohol (PVA) (1 wt % solution, Aldrich, Mw = 10,000, 80% hydrolyzed) to the solution while stirring for an extra 15 min. After this, a fresh 0.1 M NaBH4/Au 5 mol/mol was applied to the solution to develop a dark brown solution that was maintained under stirring for 30 min. Then, CNTs support was introduced to the blend and stirred for a further 1 h. The produced catalyst was recovered by filtration, rinsed with distilled water and dried for 24 h at 110 °C. The same recipe was utilized for the immobilization of Au-Pd on functionalized carbon nanotubes (O-CNT and P-CNT).

2.3. Catalyst Testing

For liquid phase epoxidation of cyclooctene and benzyl alcohol oxidation, the Radleys carousel reactor was used. Under solvent-free conditions, the fabricated Au-Pd/O-CNTs and Au-Pd/P-CNTs (200 mg) catalysts were dispersed in the substrate (2 g). The reaction blend was stirred at 1000 rpm with maintained oxygen pressure at 1 bar for the required time (6 h for cyclooctene oxidation and 2 h for benzyl alcohol oxidation) and at the required temperature (80 °C for cyclooctene oxidation and 120 °C for benzyl alcohol oxidation). Throughout the reaction, the pressure was controlled by applying a pressure gauge to prevent any changes in pressure. After a limited reaction time, a sample was withdrawn for examination applying gas chromatography (GC-Varian star CP-3800) with a CP-wax 52 column and a flame ionization detector (FID).

2.4. Catalyst Characterization

The functionalized CNTs were imaged with a scanning electron microscope (FEI, Quanta 250, Eindhoven, The Netherland) using an accelerating voltage of 15 KV and a beam spot size of 3 nm. The specimen was placed directly on double faced carbon tape. The samples imaging were performed without any metal coating. Transmission electron microscope images were obtained from Jeol 2100 instrument with a filament operating at 200 kV to assess the CNTs dispersion quality. For TEM images, the powder was suspended in methanol using ultrasonic radiation for 5 min, and a drop from the suspension was put onto the carbon-coated copper grids. The Raman studies were performed utilizing a Renishaw Raman Scope 1000 (Renishaw, Gloucestershire, UK) with 785 nm-wavelength laser. The Fourier-transform infrared FTIR spectra of the functionalized CNTs were obtained using the cary 660 FTIR spectrometer (Agilent Technologies, Santa Clara, CA, USA) and were measured in the range 200–4000 cm^{-1}.

3. Results

In order to assess the influence of the applied functionalization approaches on the structural properties of the nanotubes, Raman scattering spectra were collected for the different CNTs samples as depicted in Figure 1. The figure displays that all samples have two obvious bands at about 1350 cm^{-1} and 1570 cm^{-1} that correspond to the D band and G band of the graphite, respectively. The D-peak can be used to measure defects density in the graphitic lattice through calculating the ratio of the relative intensities of the D to the G bands. The calculated ratio was found to be about 11% and 4% higher for the oxidized CNTs and polymer functionalized CNTs, respectively, than that of the raw CNTs. The increase in the defects density in the case of the oxidized CNTs nanotubes is also much higher than that of the polymer functionalized CNTs. Such an increase in the defect density usually occurs after acid treatment of CNTs and has been confirmed in many previous studies [33–35]. These defects serve as sites for further functionalization of CNTs with chemical groups and/or nanoparticles. Additional peaks can also be seen in the figure for the polymer functionalized CNTs sample at about 1501, 1435, 1365 and 1250 cm^{-1}, which are the main peaks of the conductive PEDOT: PSS polymer, and their presence in the spectrum confirms the polymer functionalization of the CNTs. Moreover, the positions of the D and G bands in the spectrum of the polymer functionalized CNTs are slightly shifted in comparison to those of raw CNTs, which could be a result of the disorder, defect sites and changing of the CNTs diameter distribution following the polymer-CNTs interaction [36].

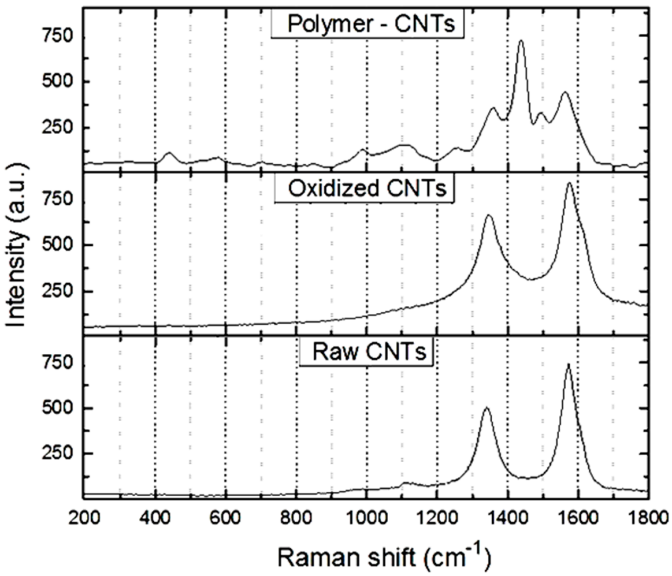


Figure 1. Raman spectra of the raw, oxidized and polymer functionalized carbon nanotubes.

FTIR spectra of raw and functionalized CNTs are presented in Figure 2. The existence of an absorption band at about 1610 cm^{-1} can be attributed to the C-C stretching in the CNTs graphitic structure [37,38]. It can also be seen from the figure that the oxidized CNTs spectrum exhibit an absorption band at about 1730 cm^{-1} corresponding to the stretching vibration of the carbonyl groups, and a broad absorption band at about 3240 cm^{-1} corresponding to OH stretching vibration band [37–39]. The presence of these absorption bands confirms the attachments of the carboxylic acid groups to the sidewalls of the CNTs. Similarly, the various absorption bands that appear in the spectrum of the polymer functionalized CNTs confirm the attachments of the polymer chains to the sidewalls of the CNTs. The absorption bands at 840, 1310 and 1521 cm^{-1} can be attributed to the C-S, C-C and C=C vibrations of the thiophene ring of PEDOT, respectively, whereas the absorption bands at 1195 cm^{-1} could be related to the SO_3H group bonding of PSS. Additional absorption bands can also be seen in the polymer functionalized CNTs spectrum at 2900 and 3350 cm^{-1}, which are mainly due to the C-H and OH stretching vibration bands, respectively [40,41].

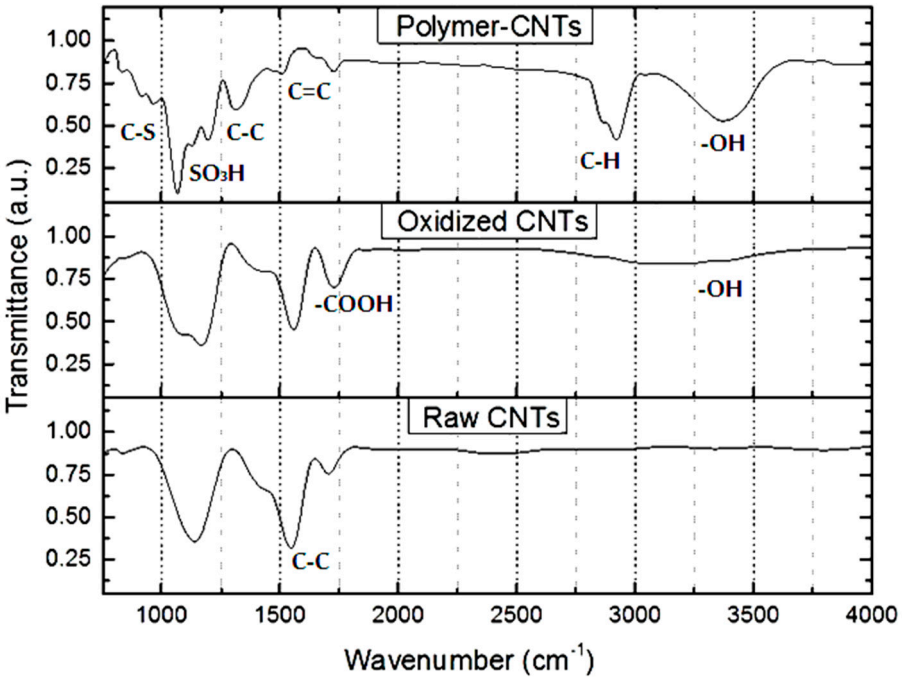


Figure 2. Fourier-transform infrared FTIR spectra of the raw, oxidized and polymer functionalized carbon nanotubes.

Nitrogen isotherms of pristine CNT and functionalized CNTs are displayed in Figure 3. The adsorption isotherms of all materials exhibit combination isotherm of type II (at greater p/p_o) and type IV adsorption (at lower p/p_o) with an H3-type hysteresis loop region of 0.9–1.0, indicating the existence of plenty of mesopores in the material. The surface areas of the CNT, O-CNT and P-CNT were found to be 200.45, 235.12 and 222.14 $m^2\ g^{-1}$, respectively, associated with an increase in the pore volume from 0.453 to 0.632 and 0.556 $cm^3\ g^{-1}$. The surface characteristics of the functionalized CNTs are higher than those of raw CNTs. This would boost the effective exposure of active sites, resulting in catalytic activity improvement.

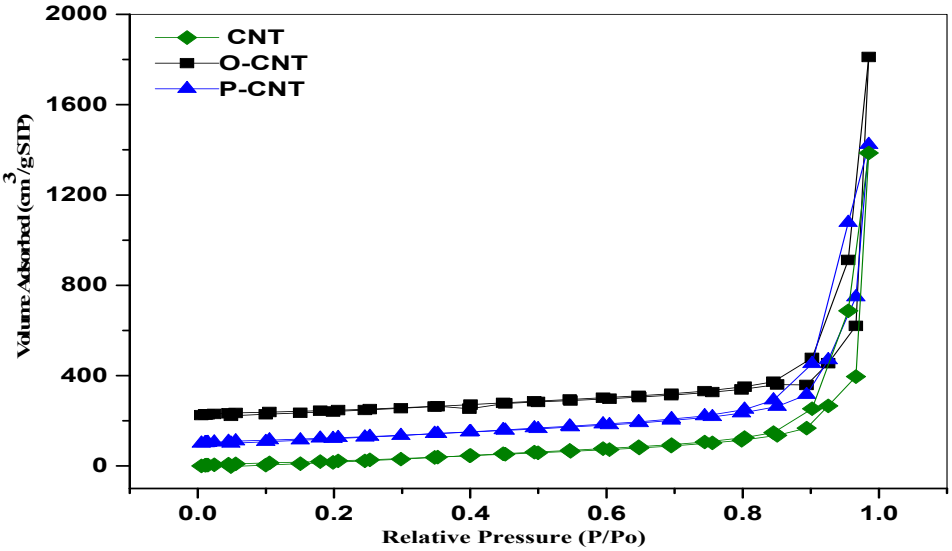


Figure 3. Nitrogen adsorption isotherms at 77 K for pristine (CNTs), oxidized (O-CNTs), and polymer functionalized (P-CNTs) nanotubes.

The scanning electron (SEM) and transmission electron (TEM) microscopes images of the oxidized and polymer functionalized CNTs are shown in Figure 4. Obviously, the figure displays the SEM images (Figure 4a,c) of both CNTs samples and show very well dispersed individual carbon nanotubes. This indicates that both used functionalization methods effectively debundled the treated nanotubes, as shown in Figure 4. These observations are also confirmed through TEM images, which also show that very good dispersion of the individual CNTs is obtained by both functionalization methods. The degree of CNTs dispersion is a very crucial factor as achieving a high degree of CNTs dispersion could greatly affect their role in chemical reactions and facilitate the attachments of additional functional groups and/or nanoparticles to their sidewalls as well [42].

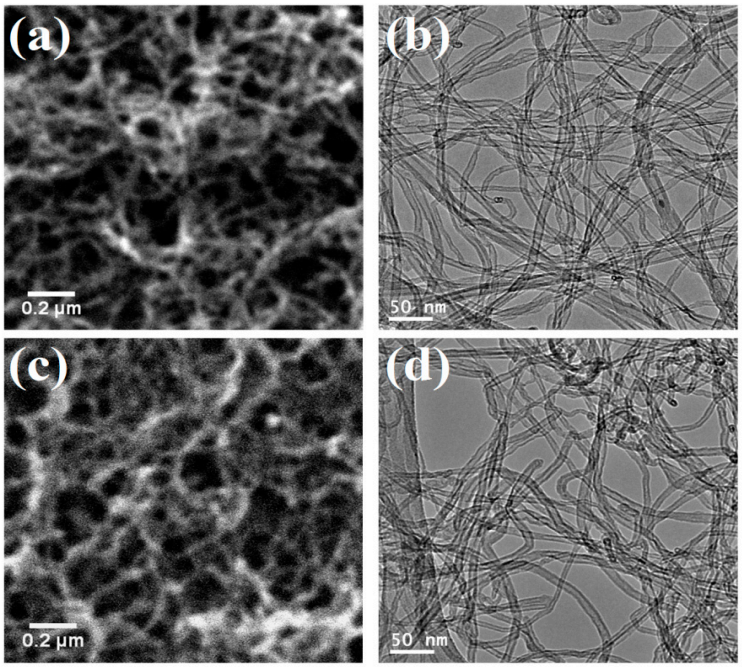


Figure 4. Scanning electron microscope images of the functionalized carbon nanotubes: (**a**) oxidized CNTs and (**c**) polymer functionalized CNTs. High resolution transmission electron microscope (HRTEM) images of the functionalized carbon nanotubes: (**b**) oxidized CNTs and (**d**) polymer functionalized CNTs.

The functionalized CNTs samples were also investigated after the attachments of the gold-palladium nanoparticles (Au-Pd NPs) by the transmission electron microscope. The TEM images of the catalysts are shown in Figure 5. As seen from Figure 5a, the existence of Au-Pd alloyed NPs on the sidewalls of the oxidized CNTs is very obvious. The Au-Pd nanoparticles are randomly distributed in the nanotubes sample and have different sizes, as shown in the magnified view of Figure 5a. Similarly, as seen from Figure 5b, the Au-Pd nanoparticles were successfully attached to the polymer functionalized CNTs as well. They exhibit random distribution as well as various nanoparticles sizes like that in the case of the oxidized CNTs but with wider particle size distribution. Moreover, no agglomeration of gold-palladium nanoparticles was observed in both samples and that can be related to the large aspect ratio of CNTs, which provide plenty of nucleation sites [43]. The average particle size was measured and found to be about 2.33 ± 0.32 nm for the nanoparticles grown on the oxidized CNTs and 2.85 ± 1.13 nm for the nanoparticles grown on the polymer functionalized CNTs as confirmed from the particle size distribution histogram (Figure 5). The small variation in the Au-Pd alloyed nanoparticles sizes in the case of the oxidized CNTs sample indicates that the grown nanoparticles are much uniform and the attached carboxylic groups to the sidewalls of the nanotubes are very suitable nucleation sites for the growth of uniform Au-Pd nanoparticles. Therefore, the oxidized CNTs can be used as a support for the growth of more uniform Au-Pd nanoparticles than polymer functionalized CNTs. These observations highlight the important role of the chemical groups attached to the CNTs sidewalls, which can be used as additional parameters to control the growth of the nanoparticles on the CNTs and their catalytic performances in various chemical reactions.

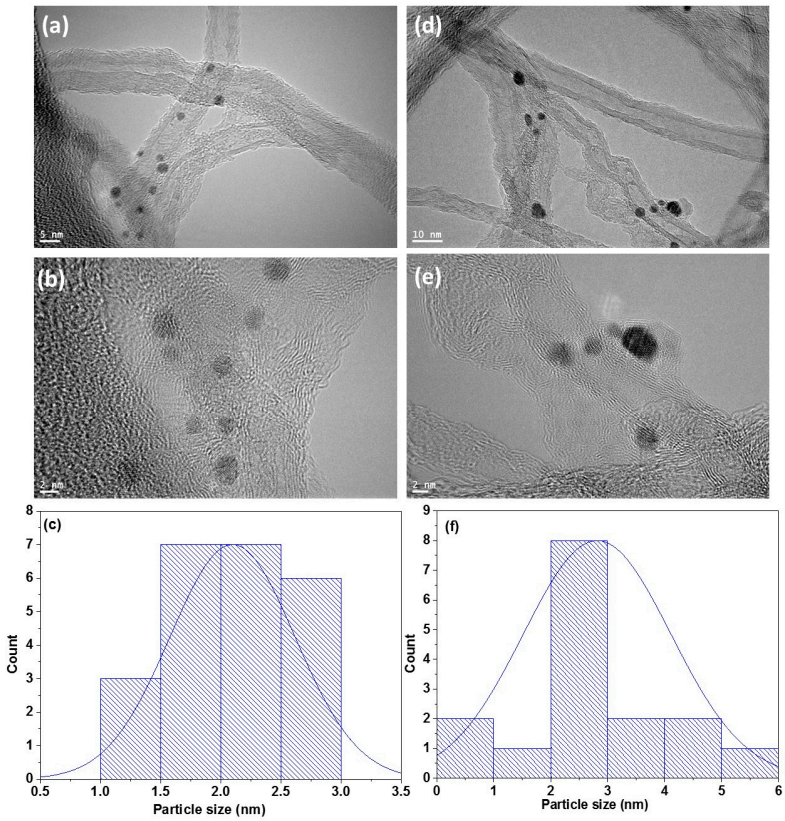


Figure 5. (**a**,**b**) High resolution transmission electron microscope (HRTEM) images and (**c**) particle size distribution histogram of the Au-Pd/ O-CNTs and (**d**,**e**) High resolution transmission electron microscope (HRTEM) images and (**f**) particle size distribution histogram of the Au-Pd/P-CNTs.

The fabricated sol-immobilized Au-Pd/O-CNTs and Au-Pd/P-CNTs catalysts were examined for the oxidation of cyclooctene (Table 1) and oxidation of benzyl alcohol (Table 2). Both reactions show that Au-Pd/O-CNTs catalysts are much more effective than Au-Pd/P-CNTs. This could be essentially attributed to the well-dispersed and smaller size of Au-Pd alloyed nanparticles, which perform as much more active sites on the surface of O-CNTs as compared to those attached to the P-CNTs surface. CNTs oxidization process contributes to the creation of several defect sites on the surface of CNTs that provide a suitable environment for the deposition of much more uniform Au-Pd alloyed nanoparticles, preventing their migration and thereby enhancing the catalyst-support interaction. This subsequently leads to the observed improvement in the catalytic efficiency of the synthesized nanocomposite materials. Besides, the difference of the selectivity of cyclooctene oxidation could be attributed to O-CNT that are richer with oxygen, which could promote the selectivity to more epoxide formation, as shown in Table 1.

Table 1. Oxidation of cyclooctene using AuPd/O-CNT and AuPd/P-CNT.

Catalyst	Conversion %	Selectivity to Epoxide %
AuPd/O-CNT	2.5	77
AuPd/P-CNT	1.7	59

Reaction conditions: 0.02 g catalyst, 1 bar of O_2, 2 g cyclooctene, 80 °C, 6 h, 2.08×10^{-4} mol *tert*-Butyl hydroperoxide (TBHP) and stirring at 1000 rpm.

Table 2. Oxidation of benzyl alcohol using Au-Pd/O-CNT and Au-Pd/P-CNT.

Catalyst	Conversion %	Selectivity to Benzyladhyde %
AuPd/O-CNT	28.3	96
AuPd/P-CNT	22.8	97.2

Reaction conditions: 0.02 g catalyst, 1 bar of O_2, 2 g benzyl alcohol, 120 °C, 2 h and stirring at 1000 rpm.

The efficiency of the fabricated catalysts Au-Pd/O-CNT and Au-Pd/P-CNT is measured in terms of the benzaldehyde selectivity in benzyl alcohol to benzaldehyde oxidation and epoxide selectivity in cyclooctene oxidation. As shown from Table 3, the bimetallic catalyst of the combination of gold with palladium immobilized on functionalized CNT shows the highest activity/selectivity combination in the cyclooctene and benzyl alcohol oxidation compared to the other catalytic materials in the literature [44–48].

Table 3. Comparison of the oxidation of benzyl alcohol and cyclooctene performance process of different catalysts.

Catalysts	Substrate	Time (h)	T °C	Solvent	Yield (%)	Reference
Au-Pd/TiO_2	Benzyl alcohol	4	80	Solvent free	6.87	[44]
Au-Pd/C	Benzyl alcohol	4	80	Solvent free	11.32	[45]
Au-Pd/CeO_2	Benzyl alcohol	3	120	Solvent free	48.8 (94.3) [a]	[46]
Au-Pd/O-CNT	Benzyl alcohol	2	120	Solvent free	28.3 (96) [a]	This work
Au-Pd/G	cyclooctene	24	80	Solvent free	2.5 (85) [b]	[47]
$Cu_3(BTC)_2$	cyclooctene	12	75	Solvent free	11(22) [b]	[48]
MWCNTs	cyclooctene	24	78	CH_3CN	3.8 (1.9)	[49]
V/MWCNTs	cyclooctene	24	48	CH_3CN	6.4 (68.4)	[49]
Au-Pd/O-CNT	cyclooctene	6	80	Solvent free	2.5 (77) [b]	This work

[a] Benzaldhyde selectivity. [b] Epoxide selectivity.

4. Conclusions

In conclusion, we developed a facile and efficient approach to prepare bimetallic nanoparticle catalysts based on the functionalization of CNTs either by oxidation or by attaching a polymer chain. The Au-Pd/O-CNTs and Au-Pd/P-CNTs catalysts were characterized and tested for the epoxidation of cyclooctene and benzyl alcohol oxidation. The functionalization and the growth of the bimetallic nanoparticles were confirmed using different morphological and optical techniques. The grown bimetallic nanoparticles on the side wall of the oxidized CNTs were found to be more uniform with a smaller size and smaller size distribution in comparison to those attached to the polymer functionalized CNTs. These observations were found to have a significant influence on the catalysts efficiency. The findings of the study also show that both oxidization reactions confirm that the Au-Pd/O-CNTs catalysts are more efficient than the Au-Pd/P-CNTs. This, in turn, highlights the importance of the defect sites produced by the functionalization process of CNTs and how they play a crucial role in controlling the growth of the bimetallic catalysts and imparting upon them such remarkable catalytic features. It also sheds light on other synthesis parameters, namely the use of functional groups, which can be used to design more efficient and high-performance metallic NPs/CNTs based catalysts. Therefore, further investigations are required to optimize CNTs functionalization processes and to explore the effect of other possible functional groups on the metallic NPs-CNTs interaction as well as their catalytic performance.

Author Contributions: H.M.A. conceived, designed the experiments and wrote the paper, A.S.A. prepared the functionalized CNTs samples and carried out the SEM, FTIR and Raman studies as well as the related results analysis, J.R.H. and S.A.A. performed the experiments, M.S.A., O.F.A. and H.M.A.H. analyzed the data; All authors contributed to the preparation of the manuscript and approved its final version. All authors have read and agreed to the published version of the manuscript.

Funding: This work was funded by the Deanship of Scientific Research (DSR), University of Ha'il under grant no. (161117).

Conflicts of Interest: The authors declare no conflict of interest.

References

1. Somorjai, G.A.; Li, Y. *Introduction to Surface Chemistry and Catalysis*; John Wiley & Sons: Hoboken, NJ, USA, 2010.
2. Guo, S.; Zhang, S.; Sun, S. Tuning nanoparticle catalysis for the oxygen reduction reaction. *Angew. Chem. Int. Ed.* **2013**, *52*, 8526–8544. [CrossRef] [PubMed]
3. Xia, Y.; Xiong, Y.; Lim, B.; Skrabalak, S.E. Shape-Controlled Synthesis of Metal Nanocrystals: Simple Chemistry Meets Complex Physics? *Angew. Chem. Int. Ed.* **2009**, *48*, 60–103. [CrossRef] [PubMed]
4. Somorjai, G.A.; Frei, H.; Park, J.Y. Advancing the frontiers in nanocatalysis, biointerfaces, and renewable energy conversion by innovations of surface techniques. *J. Am. Chem. Soc.* **2009**, *131*, 16589–16605. [CrossRef]
5. Bukhtiyarov, A.; Prosvirin, I.; Saraev, A.; Klyushin, A.Y.; Knop-Gericke, A.; Bukhtiyarov, V. In situ formation of the active sites in Pd–Au bimetallic nanocatalysts for CO oxidation: NAP (near ambient pressure) XPS and MS study. *Faraday Discuss.* **2018**, *208*, 255–268. [CrossRef] [PubMed]
6. Zhu, X.; Guo, Q.; Sun, Y.; Chen, S.; Wang, J.-Q.; Wu, M.; Fu, W.; Tang, Y.; Duan, X.; Chen, D.; et al. Optimising surface d charge of AuPd nanoalloy catalysts for enhanced catalytic activity. *Nat. Commun.* **2019**, *10*, 1–11. [CrossRef] [PubMed]
7. Chen, M.; Kumar, D.; Yi, C.-W.; Goodman, D.W. The promotional effect of gold in catalysis by palladium-gold. *Science* **2005**, *310*, 291–293. [CrossRef] [PubMed]
8. Xu, J.; White, T.; Li, P.; He, C.; Yu, J.; Yuan, W.; Han, Y.F. Biphasic Pd−Au alloy catalyst for low-temperature CO oxidation. *J. Am. Chem. Soc.* **2010**, *132*, 10398–10406. [CrossRef]
9. Gao, F.; Wang, Y.; Goodman, D.W. CO/NO and CO/NO/O_2 reactions over a Au–Pd single crystal catalyst. *J. Catal.* **2009**, *268*, 115–121. [CrossRef]
10. Gao, F.; Wang, Y.; Goodman, D.W. CO Oxidation over AuPd(100) from Ultrahigh Vacuum to Near-Atmospheric Pressures: The Critical Role of Contiguous Pd Atoms. *J. Am. Chem. Soc.* **2009**, *131*, 5734–5735. [CrossRef]

11. Herzing, A.A.; Kiely, C.J.; Carley, A.F.; Landon, P.; Hutchings, G.J. Identification of active gold nanoclusters on iron oxide supports for CO oxidation. *Science* **2008**, *321*, 1331–1335. [CrossRef]
12. Cao, L.; Liu, W.; Luo, Q.; Yin, R.; Wang, B.; Weissenrieder, J.; Soldemo, M.; Yan, H.; Lin, Y.; Sun, Z.; et al. Atomically dispersed iron hydroxide anchored on Pt for preferential oxidation of CO in H_2. *Nature* **2019**, *565*, 631–635. [CrossRef] [PubMed]
13. Qiao, B.; Wang, A.; Yang, X.; Allard, L.F.; Jiang, Z.; Cui, Y.; Liu, J.; Li, J.; Zhang, T. Single-atom catalysis of CO oxidation using Pt_1/FeO_x. *Nat. Chem.* **2011**, *3*, 634. [CrossRef]
14. Alayoglu, S.; Tao, F.; Altoe, V.; Specht, C.; Zhu, Z.; Aksoy, F.; Butcher, D.R.; Renzas, R.J.; Liu, Z.; Somorjai, G.A. Surface composition and catalytic evolution of Au_xPd_{1-x}(x= 0.25, 0.50 and 0.75) nanoparticles under CO/O_2 reaction in torr pressure regime and at 200 C. *Catal. Lett.* **2011**, *141*, 633–640. [CrossRef]
15. Liu, C.-H.; Liu, R.-H.; Sun, Q.-J.; Chang, J.-B.; Gao, X.; Liu, Y.; Lee, S.-T.; Kang, Z.-H.; Wang, S.-D. Controlled synthesis and synergistic effects of graphene-supported PdAu bimetallic nanoparticles with tunable catalytic properties. *Nanoscale* **2015**, *7*, 6356–6362. [CrossRef] [PubMed]
16. Zugic, B.; Wang, L.C.; Heine, C.; Zakharov, D.N.; Lechner, B.A.J.; Stach, E.A.; Biener, J.; Salmeron, M.; Madix, R.J.; Friend, C.M. Dynamic restructuring drives catalytic activity on nanoporous gold-silver alloy catalysts. *Nat. Mater.* **2017**, *16*, 558–564. [CrossRef] [PubMed]
17. Casanova, O.; Iborra, S.; Corma, A. Biomass into chemicals: One pot-base free oxidative esterification of 5-hydroxymethyl-2-furfural into 2, 5-dimethylfuroate with gold on nanoparticulated ceria. *J. Catal.* **2009**, *265*, 109–116. [CrossRef]
18. Taarning, E.; Nielsen, I.S.; Egeblad, K.; Madsen, R.; Christensen, C.H. Chemicals from renewables: Aerobic oxidation of furfural and hydroxymethylfurfural over gold catalysts. *ChemSusChem Chem. Sustain. Energy Mater.* **2008**, *1*, 75–78. [CrossRef]
19. Davis, S.E.; Houk, L.R.; Tamargo, E.C.; Datye, A.K.; Davis, R.J. Oxidation of 5-hydroxymethylfurfural over supported Pt, Pd and Au catalysts. *Catal. Today* **2011**, *160*, 55–60. [CrossRef]
20. Prati, L.; Martra, G. New gold catalysts for liquid phase oxidation. *Gold Bull.* **1999**, *32*, 96–101. [CrossRef]
21. Lorençon, E.; Ferreira, D.; Resende, R.; Krambrock, K. Amphiphilic gold nanoparticles supported on carbon nanotubes: Catalysts for the oxidation of lipophilic compounds by wet peroxide in biphasic systems. *Appl. Catal. A Gen.* **2015**, *505*, 566–574. [CrossRef]
22. Jawale, D.V.; Gravel, E.; Geertsen, V.; Li, H.; Shah, N.; Kumar, R.; John, J.; Namboothiri, I.N.N.; Doris, E. Size effect of gold nanoparticles supported on carbon nanotube as catalysts in selected organic reactions. *Tetrahedron* **2014**, *70*, 6140–6145. [CrossRef]
23. Oosthuizen, R.; Nyamori, V. Carbon nanotubes as supports for palladium and bimetallic catalysts for use in hydrogenation reactions. *Platin. Met. Rev.* **2011**, *55*, 154–169. [CrossRef]
24. Sheldon, R.; Kochi, J. *Metal-Catalysed Oxidations of Organic Compounds 1981*; Academic Press: New York, NY, USA, 1981.
25. Eder, D. Carbon nanotube−inorganic hybrids. *Chem. Rev.* **2010**, *110*, 1348–1385. [CrossRef]
26. Figueiredo, J.L. Functionalization of porous carbons for catalytic applications. *J. Mater. Chem. A* **2013**, *1*, 9351–9364. [CrossRef]
27. Serp, P.; Figueiredo, J.L. *Carbon Materials for Catalysis*; John Wiley & Sons: Hoboken, NJ, USA, 2009.
28. Wu, B.; Kuang, Y.; Zhang, X.; Chen, J. Noble metal nanoparticles/carbon nanotubes nanohybrids: Synthesis and applications. *Nano Today* **2011**, *6*, 75–90. [CrossRef]
29. Villa, A.; Schiavoni, M.; Prati, L. Material science for the support design: A powerful challenge for catalysis. *Catal. Sci. Technol.* **2012**, *2*, 673–682. [CrossRef]
30. Alshammari, A.S.; Alenezi, M.R.; Lai, K.T.; Silva, S.R.P. Inkjet printing of polymer functionalized CNT gas sensor with enhanced sensing properties. *Mater. Lett.* **2017**, *189*, 299–302. [CrossRef]
31. Alshammari, A.S.; Shkunov, M.; Silva, S.R.P. Correlation between wetting properties and electrical performance of solution processed PEDOT:PSS/CNT nano-composite thin films. *Colloid Polym. Sci.* **2014**, *292*, 661–668. [CrossRef]
32. Hu, H.; Zhao, B.; Itkis, M.E.; Haddon, R.C. Nitric Acid Purification of Single-Walled Carbon Nanotubes. *J. Phys. Chem. B* **2003**, *107*, 13838–13842. [CrossRef]
33. Chaturvedi, P.; Verma, P.; Singh, A.; Chaudhary, P.K.; Harsh; Basu, P.K. Carbon nanotube—Purification and sorting protocols. *Def. Sci. J.* **2008**, *58*, 591–599. [CrossRef]

34. Alshammari, H.M.; Humaidi, J.R.; Alhumaimess, M.S.; Aldosari, O.F.; Alotaibi, M.H.; Hassan, H.M.A.; Wawata, I. Bimetallic Au:Pd nanoparticle supported on MgO for the oxidation of benzyl alcohol. *React. Kinet. Mech. Catal.* **2019**, *128*, 97–108. [CrossRef]
35. Alshammari, A.S. Improved electrical stability of silver NWs based hybrid transparent electrode interconnected with polymer functionalized CNTs. *Mater. Res. Bull.* **2019**, *111*, 245–250. [CrossRef]
36. Sadegh, H.; Zare, K.; Maazinejad, B.; Shahryari-Ghoshekandi, R.; Tyagi, I.; Agarwal, S.; Gupta, V.K. Synthesis of MWCNT-COOH-Cysteamine composite and its application for dye removal. *J. Mol. Liq.* **2016**, *215*, 221–228. [CrossRef]
37. Lu, S.C.; Wang, X.Y.; Meng, Z.R.; Deng, Q.C.; Peng, F.F.; Yu, C.C.; Hu, X.; Zhao, Y.; Ke, Y.C.; Qi, F.Z. The mechanical properties, microstructures and mechanism of carbon nanotube-reinforced oil well cement-based nanocomposites. *RSC Adv.* **2019**, *9*, 26691–26702. [CrossRef]
38. Feng, M.N.; Pu, Z.J.; Zheng, P.L.; Jia, K.; Liu, X.B. Sulfonated carbon nanotubes synergistically enhanced the proton conductivity of sulfonated polyarylene ether nitriles. *RSC Adv.* **2015**, *5*, 34372–34376. [CrossRef]
39. Xiong, S.; Zhang, L.; Lu, X. Conductivities enhancement of poly (3, 4-ethylenedioxythiophene)/poly (styrene sulfonate) transparent electrodes with diol additives. *Polym. Bull.* **2013**, *70*, 237–247. [CrossRef]
40. Xu, S.; Liu, C.; Xiao, Z.; Zhong, W.; Luo, Y.; Ou, H.; Wiezorek, J. Cooperative effect of carbon black and dimethyl sulfoxide on PEDOT: PSS hole transport layer for inverted planar perovskite solar cells. *Sol. Energy* **2017**, *157*, 125–132. [CrossRef]
41. Ram, J.; Singh, R.G.; Singh, F.; Kumar, V.; Chauhan, V.; Gupta, R.; Kumar, U.; Yadav, B.C.; Kumar, R. Development of WO3-PEDOT: PSS hybrid nanocomposites based devices for liquefied petroleum gas (LPG) sensor. *J. Mater. Sci. Mater. Electron.* **2019**, *30*, 13593–13603. [CrossRef]
42. Zhang, W.W.; Li, W.L.; Wang, J.J.; Qin, C.X.; Dai, L.X. Composites of Polyvinyl Alcohol and Carbon Nanotubes Decorated with Silver Nanoparticles. *Fibers Polym.* **2010**, *11*, 1132–1136. [CrossRef]
43. Caetano, F.R.; Felippe, L.B.; Zarbin, A.J.; Bergamini, M.F.; Marcolino-Junior, L.H. Gold nanoparticles supported on multi-walled carbon nanotubes produced by biphasic modified method and dopamine sensing application. *Sens. Actuators B Chem.* **2017**, *243*, 43–50. [CrossRef]
44. Tareq, S.S.; Saiman, M.I.; Hin, T.Y.Y.; Abdullah, A.H.; Rashid, U. The impact of hydrogen peroxide as an oxidant for solvent-free liquid phase oxidation of Benzyl alcohol using Au-Pd supported carbon and titanium catalysts. *Bull. Chem. React. Eng. Catal.* **2018**, *13*, 373–385. [CrossRef]
45. Tareq, S.; Yap, Y.H.T.; Saleh, T.A.; Abdullah, A.H.; Rashid, U.; Saiman, M.I. Synthesis of bimetallic gold-pallidum loaded on carbon as efficient catalysts for the oxidation of benzyl alcohol into benzaldehyde. *J. Mol. Liq.* **2018**, *271*, 885–891. [CrossRef]
46. Li, X.; Feng, J.; Perdjon, M.; Oh, R.; Zhao, W.; Huang, X.; Liu, S. Investigations of supported Au-Pd nanoparticles on synthesized CeO_2 with different morphologies and application in solvent-free benzyl alcohol oxidation. *Appl. Surf. Sci.* **2020**, *505*, 144473. [CrossRef]
47. Alshammari, H.; Miedziak, P.J.; Knight, D.W.; Willock, D.J.; Hutchings, G.J. The effect of ring size on the selective oxidation of cycloalkenes using supported metal catalysts. *Catal. Sci. Technol.* **2013**, *3*, 1531–1539. [CrossRef]
48. Junghans, U.; Suttkus, C.; Lincke, J.; Lassig, D.; Krautscheid, H.; Glaser, R. Selective oxidation of cyclooctene over copper-containing metalorganic frameworks. *Microporous Mesoporous Mater.* **2015**, *216*, 151–160. [CrossRef]
49. Salavati-Niasari, M.; Badiei, A.; Saberyan, K. Oxovanadium(IV) salophen complex covalently anchored to multi-wall carbon nanotubes (MWNTs) as heterogeneous catalyst for oxidation of cyclooctene. *Chem. Eng. J.* **2011**, *173*, 651–658. [CrossRef]

Publisher's Note: MDPI stays neutral with regard to jurisdictional claims in published maps and institutional affiliations.

© 2020 by the authors. Licensee MDPI, Basel, Switzerland. This article is an open access article distributed under the terms and conditions of the Creative Commons Attribution (CC BY) license (http://creativecommons.org/licenses/by/4.0/).